A Quaternary Solution Model for White Micas Based on Natural Coexisting Phengite–Paragonite Pairs

L. M. KELLER*, C. DE CAPITANI AND R. ABART

DEPARTMENT OF EARTH SCIENCES, BASEL UNIVERSITY, BERNOULLISTRASSE 32, CH-4056 BASEL, SWITZERLAND

A thermodynamic model for the quaternary white mica solid solution with end-members muscovite–Mg-celadonite–paragonite–Fe-celadonite (Ms–MgCel–Pg–FeCel) is presented. The interaction energies for the MgCel–Pg join, the FeCel–Pg join and the ternary interactions were obtained from natural coexisting phengite–paragonite pairs. Phengite–paragonite pairs were selected based on the criteria that their chemical compositions may be represented as a linear combination of the model end-member compositions and that the respective formation conditions (350–650°C, 4–21 kbar) are accurately known. Previously published excess free energy expressions were used for the Ms–Pg, Ms–MgCel and Ms–FeCel binaries. The suggested mixing model was tested by calculating multicomponent equilibrium phase diagrams. This proved to be particularly well suited to reproduce compositional variations of white micas from amphibolite-facies metapelites.

INTRODUCTION

White mica is a ubiquitous phase in low- to medium-grade metamorphic pelites. In the early work of Thompson (1957) white mica was treated as an excess phase of fixed (muscovite) composition giving rise to the well-known AFM projection. It was soon recognized (Thompson, 1957; Guidotti, 1973; Thompson & Thompson, 1976) that this treatment was oversimplified in many cases, because it did not account for the compositional variations of white micas and the coexistence of potassium- and sodium-rich white micas in metapelites.

Taking muscovite as an end-member, several chemical substitutions may occur in white mica (see Fig. 1). The compositional join between the muscovite [$KAl_2(AlSi_3O_{10})(OH)_2$] and paragonite [$NaAl_2(AlSi_3O_{10})(OH)_2$] end-members is represented by the Na = K substitution. Two Tschermak-type substitutions, $SiMg = Al^{VI} + Al^{IV}$ and $SiFe^{2+} = Al^{VI} + Al^{IV}$, lead to the theoretical Mg-celadonite [$KAlMg(Si_4O_{10})(OH)_2$] and Fe-celadonite [$KAlFe(Si_4O_{10})(OH)_2$] end-members. White mica with a chemical composition along the muscovite–celadonite join is common in metapelites and is referred to as phengite. If phengite is high in sodium, the celadonite substitution is usually less pronounced (Guidottti & Sassi, 1976).

At high temperatures the muscovite–paragonite solvus tends to close, whereas at low temperatures the solvus opens and a potassium- and a sodium-rich white mica may coexist (see also Guidotti, 1984). The temperature dependence of the K–Na partitioning works well as a qualitative geothermometer, whereas its use as a quantitative geothermometer is not very successful (e.g. Guidotti & Sassi, 1976; Guidotti, 1984). Experiments showed that the solvus on the ideal Ms–Pg join widens with increasing pressure (e.g. Chatterjee & Flux, 1986). Guidotti *et al.* (1994a) showed that pressure alone cannot account for the opening of the solvus between potassium- and sodium-rich white micas, and that the celadonite component in phengite also has an influence on the Na–K partitioning between coexisting paragonite and phengite.

Since the pioneering work of Guidotti & Sassi (1976) it has been known that the solvus between sodium- and potassium-rich white micas opens with increasing celadonite content. This is documented by the fact that the phengite limb of the solvus approaches successively more potassium-rich compositions with increasing

*Corresponding author. Telephone: 0041/(0) 61 267 36 31. Fax: 0041/(0) 61 267 36 13. E-mail: Lukas.Keller@unibas.ch
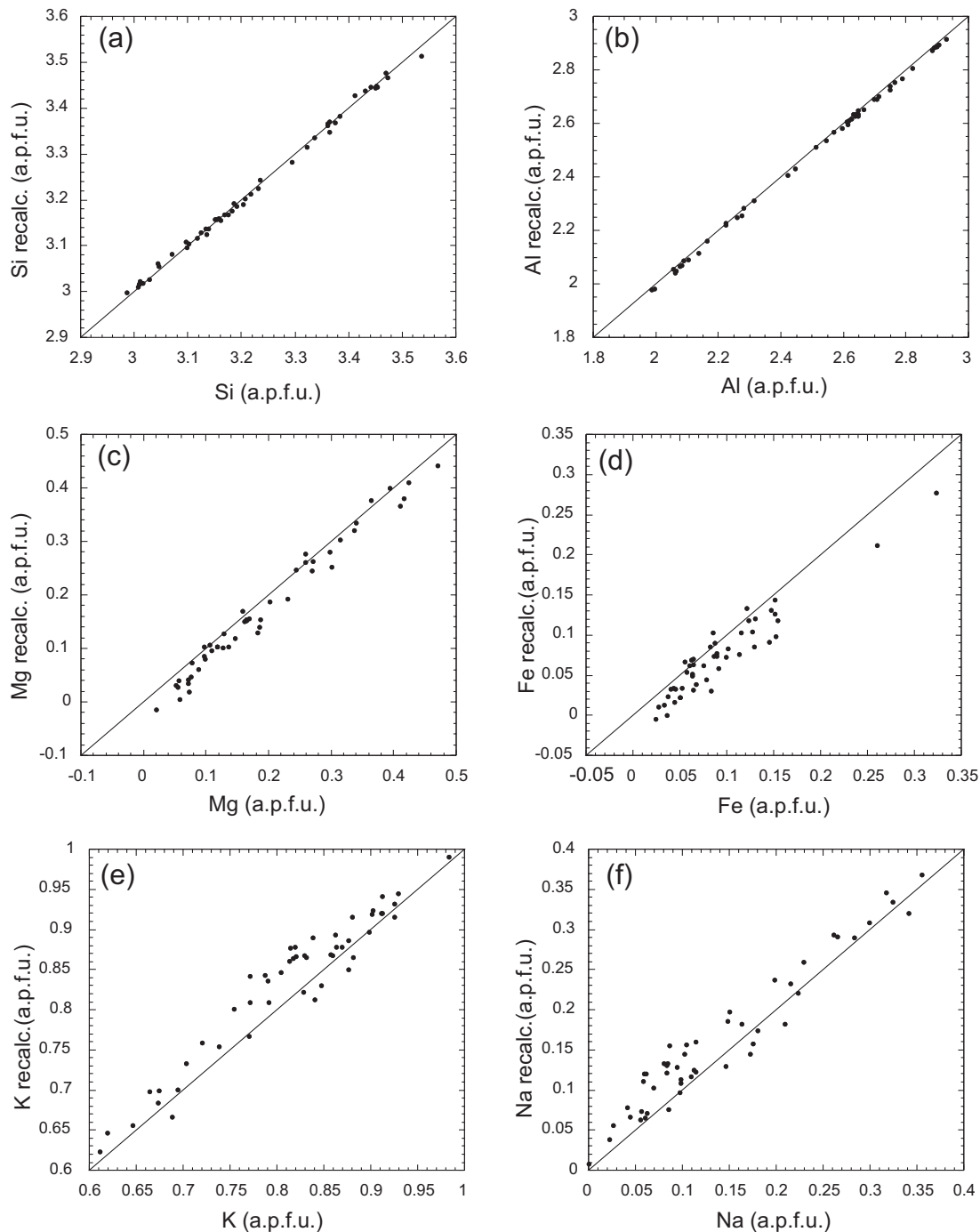
Fig. 1. Correlation between chemical composition of phengite and its recalculated composition. The measured content of Si (a), Al (b), Mg (c), Fe (d), K (e) and Na (f) (a.p.f.u.) is plotted vs the recalculated contents assuming that phengite is a linear combination of four end-members. An analysis representing an ideal linear combination of the four considered end-members should lie on the diagonal lines.

celadonite component (Katagas & Baltazis, 1980; Enami, 1983; Grambling, 1984; Guidotti, 1984). The celadonite content in phengite, in turn, increases with increasing pressure but is also sensitive to mineral assemblage (Guidotti & Sassi, 1998).

Mixing models exist for the binary muscovite–paragonite (Eugster *et al.*, 1972; Chatterjee & Froese, 1975; Chatterjee & Flux, 1986; Roux & Hovis, 1996) and the muscovite–celadonite joins (Massonne & Szpurka, 1997; Coggon & Holland, 2002). A quaternary

model, which covers the entire composition space that spans the muscovite, paragonite, Mg-celadonite and Fe-celadonite end-members, has, however, not been calibrated so far.

We suggest a quaternary mixing model that covers a major part of the composition space of phengite and paragonite. Our model is based on existing binary interaction parameters from the literature and additional binary and ternary interaction terms, which were derived from the analysis of coexisting phengite and paragonite from natural rocks. Our model accounts for the combined pressure and bulk-rock composition effect on the K–Na partitioning between coexisting Phe and Pg. Application of our model in phase equilibrium calculations yields reasonable descriptions of phase relations in metapelites and will foster the petrological analysis of white mica-bearing assemblages by means of geothermobarometry and phase diagram calculations. This particularly concerns pelitic schists at high-pressure metamorphic conditions where sodium and potassium are mainly stored within Phe and Pg.

INPUT DATA
Published solid solution models based on experimental data

The shape of the solvus in the quaternary white mica system strongly depends on the three binary solvi along the Ms–Pg, Pg–MgCel and Pg–FeCel joins. At low-temperature conditions, each of the three binary joins exhibits miscibility gaps. It is found that the Ms–Pg solid solution model of Roux & Hovis (1996) best fits the compositional data from our samples. This is particularly true for pairs of coexisting Phe–Pg from Al-rich high-grade ($\approx 600°$C, ≈ 7 kbar) pelitic rocks from the Lepontine Alps. The model of Roux & Hovis (1996) predicts a relatively narrow miscibility gap. The miscibility gap of solution models from earlier workers (e.g. Chatterjee & Froese, 1975) is too wide to reproduce natural data (Blencoe *et al.*, 1994, fig. 3; Roux & Hovis, 1996). For the two binaries Ms–MgCel and Ms–FeCel we used the solution model of Massonne & Szpurka (1997).

End-member calculation of natural coexisting paragonite–phengite pairs

We investigated 63 pairs of coexisting Pg–Phe from 56 samples (Table 1). Data were taken from the literature and from our own work. With the exception of references 1, 7, 10, 17, 18, 23 and 25 the data sources listed in Table 1 were also used by Guidotti *et al.* (1994*a*, table 1) for analysing the effect of the ferromagnesian components on the paragonite–muscovite solvus. Sample selection was based on the following criteria. (1) The *P–T*

conditions of Pg–Phe equilibration must be known accurately. For the data taken from Guidotti *et al.* (1994*a*, table 1) we used their *P–T* estimates as conditions of Pg–Phe equilibration. (2) The chemical composition of the white micas must be a linear combination of the end-members Ms, Pg, MgCel and FeCel.

The mole fractions of the end-members Ms, Pg MgCel and FeCel were calculated by applying the method of least squares to the following set of equations:

$$\begin{bmatrix} 3 & 3 & 4 & 4 \\ 3 & 3 & 1 & 1 \\ 0 & 0 & 0 & 1 \\ 0 & 0 & 1 & 0 \\ 1 & 0 & 1 & 1 \\ 0 & 1 & 0 & 0 \end{bmatrix} \begin{bmatrix} X_{Ms} \\ X_{Pg} \\ X_{MgCel} \\ X_{FeCel} \end{bmatrix} = \begin{bmatrix} Si \\ Al \\ Fe \\ Mg \\ K \\ Na \end{bmatrix}$$

where the matrix to the left contains the stoichiometric coefficients of Si, Al, Fe, Mg, K, and Na in end-member compositions (columns), and the column vector on the right-hand side gives the measured white mica composition. X_{Ms}, X_{Pg}, X_{MgCel} and X_{FeCel} are the end-member mole fractions. The element concentrations of each sample were recalculated from the end-member contents and compared with the element concentrations analysed by electron microprobe. Theoretically there should be a 1:1 correlation between recalculated and analysed element concentrations. In actual fact, small discrepancies between analysed and recalculated element concentrations occur. On the one hand, these discrepancies may reflect the analytical uncertainty inherent in microprobe analysis and, on the other hand, they may be due to the fact that the four end-members cannot fully account for white mica compositions. Assuming that the deviation of the recalculated element concentrations from the analysed ones is normally distributed, we calculated the 1σ standard deviation for each element. In our analyses we only considered those samples that fall within a 3σ band around the 1:1 correlation for each element [3σ (atoms per formula unit; a.p.f.u.) is 0·066 for Si, 0·025 for Al, 0·056 for Fe, 0·054 for Mg, 0·083 for K, 0·086 for Na]. Based on this criterion 14 Phe–Pg pairs were excluded. Of the remaining 49 Phe–Pg pairs only 40 were used for the calibration of a mixing model. The following nine pairs were only used for comparative purposes and model testing: (1) three pairs from Nagel (2002), for which *P–T* conditions of equilibration are uncertain; (2) the five Phe–Pg pairs (X_{FeCel} in phengite $\leq 0·01$, X_{MgCel} in phengite $\leq 0·05$) with high Na in phengite (X_{Pg} in phengite 0·29–0·37) of Irouschek (1983), which have almost ideal binary composition and thus are used to test the solvus close to the Ms–Pg join only; (3) one pair for which phengite composition gives negative end-member values.

Table 1: Source of data and P–T *conditions of coexisting phengite and paragonite pairs*

Sample	T (°C)	P (kbar)	Ref.	n
Low-T, low-P				
71a	350	4−6*	1	2
140c	350	4−6*	1	2
187c	350	4−6*	1	2
764 MR	350	5	2	2
51/57	450−500†	>7†	3	2
114/70	450−500†	>7†	3	2
157/70	450−500†	>7†	3	2
131/70	450−500†	>7†	3	2
33-1H	480−500	7	4	2
33-5A	480−500	7	4	2
34-3A	480−500	7	4	2
3-6A	480−500	7	4	2
8-6A	480−500	7	4	2
26-3B	480−500	7	4	2
39-3A	480−500	7	4	2
?	425†	8·9†	5	2
Total				32
Low-T, medium-P				
23th	420	>11	6	2
Cere0041	365	13	7	4
AL269	510	13·5	8	2
P80/36	450	17	9	2
P82/46	450	17	9	2
6·298c	420‡	14‡	10	2
Total				14
High-T, low-P				
77-244c	580†	4†	11	2
81-42	580†	4†	11	2
M.76.2W	530	5	12	2
A271	580−610†	6†	13	2
A40	580−610†	6†	13	2
510	580−610†	6†	13	2
T10	600	7	14	2
KL264	600	7	14	2
KL285	600	7	14	2
KL185	600	7	14	2
KL98	600	7	14	2
AI 235	625	<7	15	2
AI 280	625	<7	15	2
AI 286	625	<7	15	2
AI 389	625	<7	15	2
AI 365	625	<7	15	2
Total				32

Table 1: continued

Sample	T (°C)	P (kbar)	Ref.	n
High-T, medium-P				
OP-08	∼600	∼10	16	2
CHM1	∼650	10−11	17	2
3	650	12·5	18	6
4	650	12·5	18	10
PD-162	520−580	10−13	19	2
PD-167A	520−580	10−13	19	2
PD-189C	520−580	10−13	19	2
Ad85	>550	>15	20	2
88DM143	500−600	15	21	2
3 M	600	15	22	2
KL283	600−700*	9−15*	23	2
KL409	600−700*	9−15*	23	2
Total				36
High-T, high-P				
Z6-50-12	<700	18−21	17	2
24-23	580−640	18−24	24	2
43-3	580−640	18−24	24	2
82092801	580−640	18−24	24	2
KL264	>580*	>17*	23	2
92-17A	600−650	20·5−21·5	25	2
Total				12
Overall sum				126

1, Katagas & Baltatzis (1980); 2, Franceschelli *et al*. (1989); 3, Höck (1974); 4, Ferry (1992); 5, Ahn *et al*. (1985); 6, Gil Ibarguchi & Dallmeyer (1991); 7, S. Bucher (unpublished data and personal communication, 2003); 8, Okay (1989); 9, Theye & Seidel (1991); 10, Chopin (1979); 11, Grambling (1984); 12, Ashwhorth & Evirgen (1984); 13, Hoffer (1978); 14, Koch (1982); 15, Irouschek (1983); 16, Enami (1983); 17, Meyre *et al*. (1999); 18, Keller *et al*. (2005); 19, Feininger (1980); 20, Heinrich (1982); 21, Chopin *et al*. (1991); 22, Brown & Forbes (1986); 23, Nagel (2002); 24, Hirajima *et al*. (1988); 25, Zhang & Liou (1994).
*P and/or T after the present author.
†P and/or T after Guidotti *et al*. (1994a).
‡P and T after Vidal *et al*. (2001).

Phengite composition

For phengite, the measured chemical compositions are compared with the compositions recalculated from the end-members in Fig. 1. Figure 2a shows that in our dataset X_{Cel} ($X_{\text{MgCel}} + X_{\text{FeCel}}$) in Phe is correlated with the Si content. This indicates that the Si content is predominantly controlled by the Tschermak substitution $(\text{SiMg/Fe}^{2+} = \text{Al}^{\text{VI}} + \text{Al}^{\text{IV}})$. The pyrophyllitic substitution $[(\text{Na/K})\text{Al} = \square\text{Si}]$ (e.g. Bousquet *et al*., 2002) has only a minor effect on the Si content in Phe. This is supported by the fact that the generally high K + Na
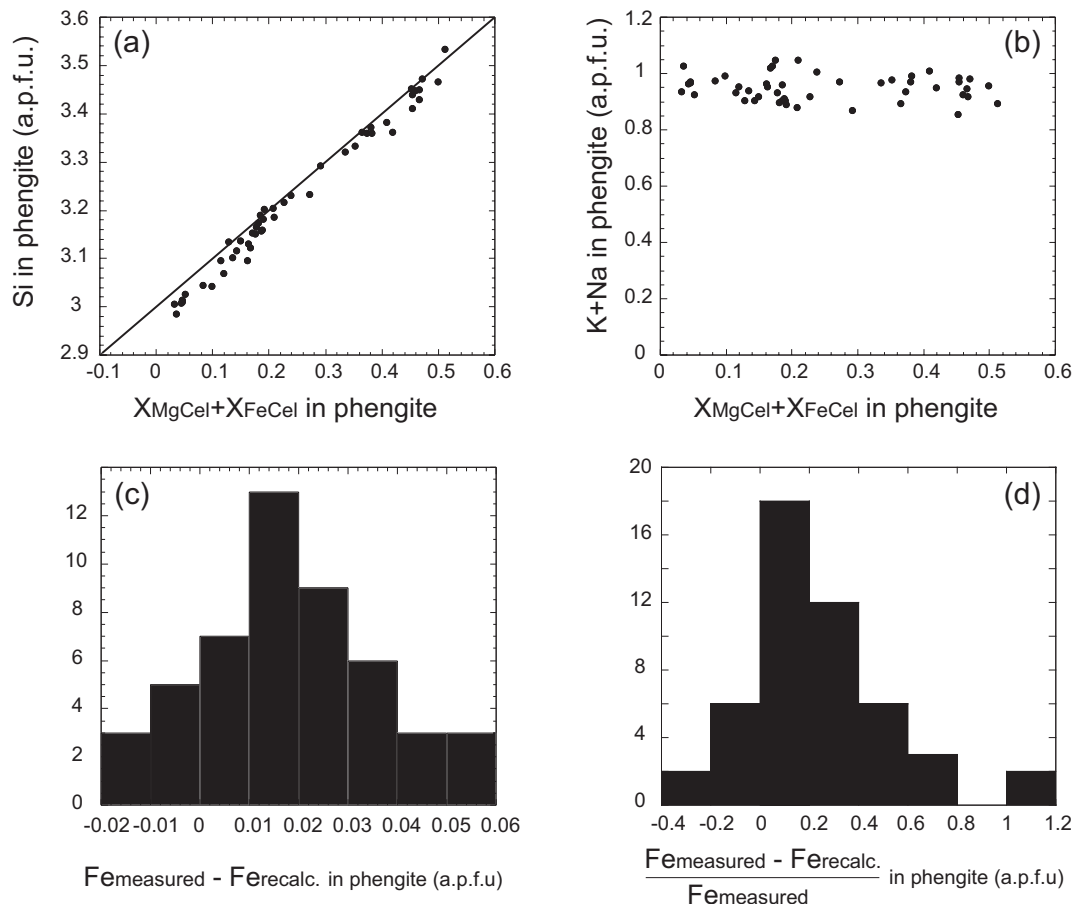
Fig. 2. (a) Si content of phengite vs calculated celadonite content. An analysis that represents a ideal linear combination of the four considered end-members, and that results from true Tschermak substitution, should lie along the diagonal line. (b) K + Na content of phengite vs calculated celadonite content. If the Si content in phengite is also controlled by pyrophyllitic substitution there should be a dependence between the K + Na content of phengite and celadonite content. (c) Frequency diagram of the difference between the measured and the recalculated Fe content in phengite (a.p.f.u.). For further explanation the reader is referred to the text. (d) Frequency diagram of the ratios between the difference between the measured and the recalculated Fe content and the measured Fe content in phengite. For further explanation the reader is referred to the text.

content in Phe does not depend on X_{Cel} ($X_{MgCel} + X_{FeCel}$) (Fig. 2b). The recalculated Mg content in Phe shows fairly good correlation with the measured Mg content (Fig. 1c). In contrast, the recalculated Fe content of Phe is systematically lower than the measured Fe content (Fig. 1d). This discrepancy suggests that most of the selected phengites contain ferric iron. Assuming that the deviation between the analysed and recalculated Fe contents reflects the ferric iron content its maximum is ≈ 0.06 Fe^{3+} a.p.f.u., and most analyses of phengite contain less than ≈ 0.04 Fe^{3+} a.p.f.u. (Fig. 2c). The ferric to ferrous iron ratio of most phengites does not exceed ≈ 0.6. Nevertheless, fairly high Fe^{3+} contents are indicated for some samples (Fig. 2d). For two out of the five almost binary samples of Irouschek (1983) the Fe^{3+} content is up to the total Fe (0.02 and 0.04 a.p.f.u.) (Fig. 2d). *In situ* measurements (XANES) of the ferric iron content in ultrahigh-pressure eclogites reveal ferric–ferrous ratios in phengite

in the range of 0.2–0.6 (Schmid *et al.*, 2003). Hence, there is agreement between the magnitude of measured ferric–ferrous ratios and those suggested from stoichiometric considerations. A good correlation between the measured and the recalculated Al content is observed. This suggests that the Fe^{3+} content of the selected phengites does not result from the substitution of $(Fe^{3+})^{VI}$ for Al^{VI}. Possibly the Fe^{3+} content in the phengites can be explained by the substitution $Fe^{2+} + H = Fe^{3+} + \square$ (see Guidotti, 1984). In addition, Fig. 1c and d indicates that phengite is generally higher in Mg than in Fe. Apparently the substitution $SiMg = Al^{VI} + Al^{IV}$ is preferred to the substitution $SiFe^{2+} = Al^{VI} + Al^{IV}$, particularly in phengite with high Si content.

Paragonite composition

It has repeatedly been reported (Guidotti, 1984) that, in contrast to phengite, paragonite generally contains very

little or no Mg, Fe^{2+} or Fe^{3+}. Guidotti *et al.* (2000) reported that the incorporation of minor amounts of these cations into paragonite does not depend on pressure. Substitution of substantial amounts of magnesium and ferric or ferrous iron would destabilize paragonite as a result of crystallochemical constraints (Guidotti, 1984). In addition, it was shown experimentally that magnesium substitution is very limited in paragonite (Franz & Althaus, 1976). These findings are in line with our observations. In our dataset the average Mg content is 0·015 ($\sigma = 0\cdot011$) a.p.f.u. and the average $Fe_{tot.}$ content is 0·024 ($\sigma = 0\cdot016$) a.p.f.u.

CALCULATION PROCEDURE

In the quaternary system Ms–MgCel–Pg–FeCel we estimated the binary interaction parameters on the MgCel–Pg and on the FeCel–Pg joins, and all ternary interaction parameters from the available information on compositions and formation conditions of coexisting Pg–Phe pairs (Table 1). The remaining interaction parameters were taken from published solution models (see above).

Chemical potential expression

If the quaternary solutions are described in terms of their end-members, the following expression gives the Gibbs free energy as a function of the respective end-member concentrations, where ΔG_{ex} accounts for molecular non-ideal mixing:

$$\Delta G_{mix} = \sum_{i}^{n} x_i \mu_i^o + RT \sum_{i}^{n} x_i \ln x_i + \Delta G_{ex} \qquad (1)$$

where μ_i^o is the chemical potential of end-member i at standard state and X_i is the mole fraction of end-member i ($i = 1$ for Ms; 2 for MgCel; 3 for Pg; 4 for FeCel).

For ΔG_{ex} we used the quaternary expansion of Jackson (1989), which is based on the ternary equation of Wohl (1946, 1953). The following relation gives the quaternary excess function (ΔG_{ex}):

$$\Delta G_{ex} = X_1 X_2 (X_1 W_{112} + X_2 W_{122})$$
$$+ X_1 X_3 (X_1 W_{113} + X_3 W_{133})$$
$$+ X_1 X_4 (X_1 W_{114} + X_4 W_{144})$$
$$+ X_2 X_3 (X_2 W_{223} + X_3 W_{233})$$
$$+ X_2 X_4 (X_2 W_{224} + X_3 W_{244})$$
$$+ X_3 X_4 (X_3 W_{334} + X_4 W_{344})$$
$$+ X_1 X_2 X_3 Q_{123} + X_1 X_2 X_4 Q_{124}$$
$$+ X_1 X_3 X_4 Q_{134} + X_2 X_3 X_4 Q_{234} \qquad (2)$$

where

$$Q_{ijk} = 0\cdot5(W_{i-j} + W_{j-i} + W_{i-k} + W_{k-i}$$
$$+ W_{j-k} + W_{k-j}) - C_{ijk}. \qquad (3)$$

In our treatment we set the ternary Wohl C_{ijk} terms to zero. Because there are no indications of an asymmetric miscibility gap between MgCel–Pg and between FeCel–Pg, a symmetric Margules mixing model was used for these binary joins ($W_{223} = W_{233}$, $W_{334} = W_{344}$). We assume ideal Fe–Mg mixing on the MgCel–FeCel binary join (Coggon & Holland, 2002) thus W_{224} and W_{244} are set to zero. These simplifications yield an excess function:

$$\Delta G_{ex} = X_1 X_2 (X_1 W_{112} + X_2 W_{122})$$
$$+ X_1 X_3 (X_1 W_{113} + X_3 W_{133})$$
$$+ X_1 X_4 (X_1 W_{114} + X_4 W_{144})$$
$$+ X_2 X_3 (X_2 W_{223} + X_3 W_{233})$$
$$+ X_3 X_4 (X_3 W_{334} + X_4 W_{344})$$
$$+ X_1 X_2 X_3 (0\cdot5 W_{112} + 0\cdot5 W_{122}$$
$$+ 0\cdot5 W_{113} + 0\cdot5 W_{133} + 0\cdot5 W_{223} + 0\cdot5 W_{233})$$
$$+ X_1 X_2 X_4 (0\cdot5 W_{112} + 0\cdot5 W_{122}$$
$$+ 0\cdot5 W_{114} + 0\cdot5 W_{144})$$
$$+ X_1 X_3 X_4 (0\cdot5 W_{113} + 0\cdot5 W_{133} + 0\cdot5 W_{114}$$
$$+ 0\cdot5 W_{144} + 0\cdot5 W_{334} + 0\cdot5 W_{344})$$
$$+ X_2 X_3 X_4 (0\cdot5 W_{223} + 0\cdot5 W_{233}$$
$$+ 0\cdot5 W_{334} + 0\cdot5 W_{344}). \qquad (4)$$

The binary interaction parameters W_{112}, W_{122}, W_{114}, W_{144}, W_{113} and W_{133} were taken from the literature (Roux & Hovis, 1996; Massonne & Szpurka, 1997). As we assumed symmetric mixing between MgCel–Pg and between FeCel–Pg there remain two unknown parameters in equation (4): W_{223} ($= W_{233}$) and W_{334} ($= W_{344}$).

The chemical potentials can be calculated from the relation

$$\mu_m = \Delta G_{mix} + \frac{\partial \Delta G_{mix}}{\partial x_m} - \sum_{i=1}^{n} x_i \frac{\partial \Delta G_{mix}}{\partial x_i} \qquad (5)$$

where μ_m is the chemical potential of any end-member. The second term in (5) is given by the expression

$$\frac{\partial \Delta G_{mix}}{\partial x_m} = \mu_m^o + RT \ln x_m + RT + \frac{\partial \Delta G_{ex}}{\partial x_m} \qquad (6)$$

and the third term in (5) is given by

$$\sum_{i=1}^{n} x_i \frac{\partial \Delta G_{mix}}{\partial x_i} = \sum_{i=1}^{n} \mu_i^o x_i + RT \sum_{i=1}^{n} x_i \ln x_i$$
$$+ RT \sum_{i=1}^{n} x_i + \sum_{i=1}^{n} x_i \frac{\partial \Delta G_{ex}}{\partial x_i} \qquad (7)$$

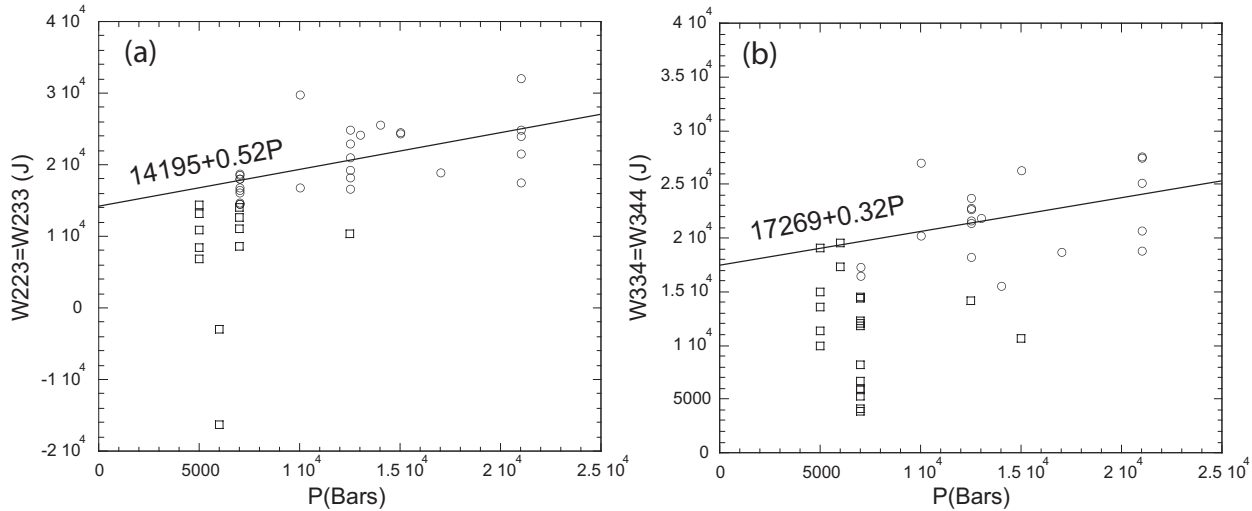by considering

$$RT \sum_{i=1}^{n} x_i = RT \qquad (8)$$

Fig. 3. Calculated interaction energies vs pressure and the resulting fit of the interaction parameters. $\bigcirc$, Interaction energies used to fit the interaction parameters; $\square$, omitted interaction energies. It should be noted that at ≤ 7000 bar pressure the calculated interaction energies scatter over a wide range and do not linearly depend on pressure. (a) Interaction energies and parameters for the binary paragonite–Mg-celadonite join. (b) Interaction energies and parameters for the binary paragonite–Fe-celadonite join.

and combining (1), (3), (4) and (5) the chemical potential can be expressed as

$$\mu_m = \mu_m^\circ + RT \ln x_m + \Delta G_{\mathrm{ex}} + \frac{\partial \Delta G_{\mathrm{ex}}}{\partial x_m} - \sum_{i=1}^{n} x_i \frac{\partial \Delta G_{\mathrm{ex}}}{\partial x_i}. \tag{9}$$

Then for the quaternary system at a given P and T, two coexisting Phe–Pg pairs must meet the following equilibrium conditions:

$$\begin{aligned}
\mu_{\mathrm{Ms}}^{\mathrm{Phe}} &= \mu_{\mathrm{Ms}}^{\mathrm{Pg}} \\
\mu_{\mathrm{MgCel}}^{\mathrm{Phe}} &= \mu_{\mathrm{MgCel}}^{\mathrm{Pg}} \\
\mu_{\mathrm{Pg}}^{\mathrm{Phe}} &= \mu_{\mathrm{Pg}}^{\mathrm{Pg}} \\
\mu_{\mathrm{FeCel}}^{\mathrm{Phe}} &= \mu_{\mathrm{FeCel}}^{\mathrm{Pg}}.
\end{aligned} \tag{10}$$

By substituting the derivations of equation (4) into equation (9), which is subsequently substituted into equations (10) and collecting all unknown parameters, one obtains a system of four equations with two unknowns. The unknown interaction energies W_{223} $(= W_{233})$ and W_{334} $(= W_{344})$ for 40 selected pairs of coexisting Phe–Pg were calculated at the corresponding P–T conditions by applying the method of least squares to the system of equations (10). From the pressure dependence of the obtained interaction energies we fitted W_{V} for the unknown interaction parameters. A temperature-dependent term W_{s} was not considered. This is motivated by the fact that the shift of the Phe-limb of the solvus can be correlated to a pressure-induced increase of the ferromagnesian content of Phe (Guidotti *et al.*, 1994*a*) indicating that the non-ideality of the Phe–Pg solvus depends primarily on pressure and not on temperature.

When minerals with close to end-member compositions are used, the calculated interaction energies are very sensitive to uncertainties in the determination of end-member contents. In this respect, the celadonite content in paragonite poses a problem, because the mole fractions of X_{MgCel} and X_{FeCel} in paragonite are generally small. To avoid this problem, a constant value for X_{MgCel} and X_{FeCel} in paragonite was assumed for all the phengite–paragonite pairs that were used for the calculation of interaction energies. The mean celadonite content of the 49 paragonites is 1·2 mol %, whereas the average proportion of Fe- and Mg-celadonite is 0·63. On average this yields 0·7 mol % Mg-celadonite and 0·5 mol % for Fe-celadonite contents in paragonite. The major problem of fitting the interaction parameters on the MgCel–Pg join and the FeCel–Pg join is the lack of data on Phe with compositions near both binary joins. However, the calculated interaction energies for the MgCel–Pg join (W_{223}, W_{233}) and the FeCel–Pg join (W_{334}, W_{344}), in particular for coexisting Phe–Pg pairs, for which the celadonite content in phengite is high, cause a miscibility gap at corresponding P–T conditions. Consequently we used binary interaction energies, which are high enough to produce miscibility gaps in order to fit for both W_{223} $(=W_{233})$ and W_{334} $(=W_{344})$ (open circles in Fig. 3a and b). It should be noted that the binary interaction energies used correspond to Phe–Pg pairs equilibrated at ≥ 7 kbar where the interaction energy is a linear function of pressure. Below 7 kbar the calculated interaction energies scatter over a wide range and most

Table 2: Margules excess terms, for the system Ms–MgCel–Pg–FeCel

	W_H (J)	W_S (J/K)	W_V (J/bar)
W_{112}*		15·920	0·187
W_{122}*		58·598	0·735
W_{113}†	6150		0·452
W_{133}†	15050		0·452
W_{114}* $= W_{144}$*		24·083	0·3394
$W_{223} = W_{233}$	**14195**		**0·520**
$W_{334} = W_{344}$	**17269**		**0·320**
$W_{123} = Q_{123}$	**24795**	**37·260**	**1·430**
$W_{124} = Q_{124}$		**61·340**	**0·800**
$W_{134} = Q_{134}$	**27869**	**24·083**	**1·111**
$W_{234} = Q_{234}$	**31464**		**0·840**

Note: $W_G = W_H - W_S T + W_V P$. Parameter labelling after equation (2). The bold values are estimated by this study.
*Excess terms after Massonne & Szpurka (1997).
†Excess terms after Roux & Hovis (1996).

interaction energies are too small to produce miscibility gaps. The determined and used values for the Margules parameters are listed in Table 2.

COMPARISON BETWEEN THE MODEL PREDICTIONS AND OBSERVATIONAL DATA

To test our model, we recalculated the phengite composition of the 40 pairs of coexisting Phe–Pg that we used to derive interaction energies. In addition, we compared model predictions and measured compositions for the samples of Irouschek (1983). The thermodynamic calculations were done with the program THERIAK (De Capitani & Brown, 1987; De Capitani, 1994), which calculates the stable mineral assemblage and the composition of the solid solutions for fixed values of P, T and given bulk composition. In this case the stable mineral assemblage is always composed of Phe and Pg. For the bulk composition we used the composition defined by a 1:1 mixture of the measured compositions of the coexisting phengite and paragonite. The results and 2σ of the difference between the reference composition and the calculated composition are given in Fig. 4. The good correlation between measured and recalculated compositions in Fig. 4 shows that the model correctly reflects white mica phase relations. THERIAK is based on a G-minimization algorithm, which computes chemical equilibria in complex systems containing non-ideal solutions. For more details the reader is referred to the homepage of the THERIAK-DOMINO-THERTER

software at http://titan.minpet.unibas.ch/minpet/theriak/theruser.html.

To further test our model we calculated isothermal and isobaric sections of the ternary Phe–Pg (Ms–MgCel–Pg) miscibility gap and compared these with natural data (Fig. 5). For the sake of simplicity, data points that lie inside the quaternary composition space are projected onto the Ms–MgCel–Pg ternary plane from the FeCel apex. Because this projection deviates from a thermodynamic projection, and to obtain an idea of the geometry of the quaternary solvus, we also projected sectional parts of the quaternary Phe–Pg (Ms–MgCel–Pg–FeCel) miscibility gap onto the Ms–MgCel–Pg ternary plane; the sections correspond to a constant X_{FeCel} in phengite.

To illustrate the effect of P and T on the ternary solvus, calculations were carried out for five P–T regimes. The pairs of coexisting phengite–paragonite were divided into five P–T categories (Table 1, Fig. 5). The ternary sections were calculated with the program THERTER (De Capitani, 1994) using the thermodynamic end-member properties for Ms, MgCel and Pg of Berman (1988, update 1992). Because the solvus varies only slightly within the P–T range of a distinct P–T category the sections were calculated for the lower and upper P–T boundary limiting the categories (Fig. 5). Figure 5 shows that our model is compatible with most of the selected 49 Phe–Pg pairs.

The effect of the Cel component on the Phe–Pg solvus is most pronounced at high-T and low-P conditions, and only if X_{MgCel} in Phe is relatively low ($X_{MgCel} < 0.2$) (Fig. 5b). Towards lower temperatures the above effect decreases (Fig. 5a and b). As pressure increases the solvus widens and consequently the effect of the MgCel component becomes less pronounced (Fig. 5c and d).

COMPARING OUR SOLUTION MODEL WITH OTHER MODELS, APPLICATION AND DISCUSSION
Comparing our solution model with other models

Because the effect of the MgCel component on the Phe–Pg solvus is most pronounced for low MgCel contents in Phe we compare our model with the Pg–Ms solvus established by Guidotti *et al.* (1994*b*). Those workers used pairs of natural coexisting Pg–Ms with compositions (Fig. 6a, Guidotti *et al.*, 1994*b*, table A1) near the ideal Pg–Ms join to establish parametric equations that describe the T–X form of the solvus. The Ms compositions used by Guidotti *et al.* (1994*b*) deviate slightly from the end-member composition of muscovite [Fig. 6a, Si 3·0–3·14 a.p.f.u; Fm ($Fe^{2+} + Mg + Fe^{3+}$) = 0·02–0·26 a.p.f.u.]. To compare predictions from our model with the model
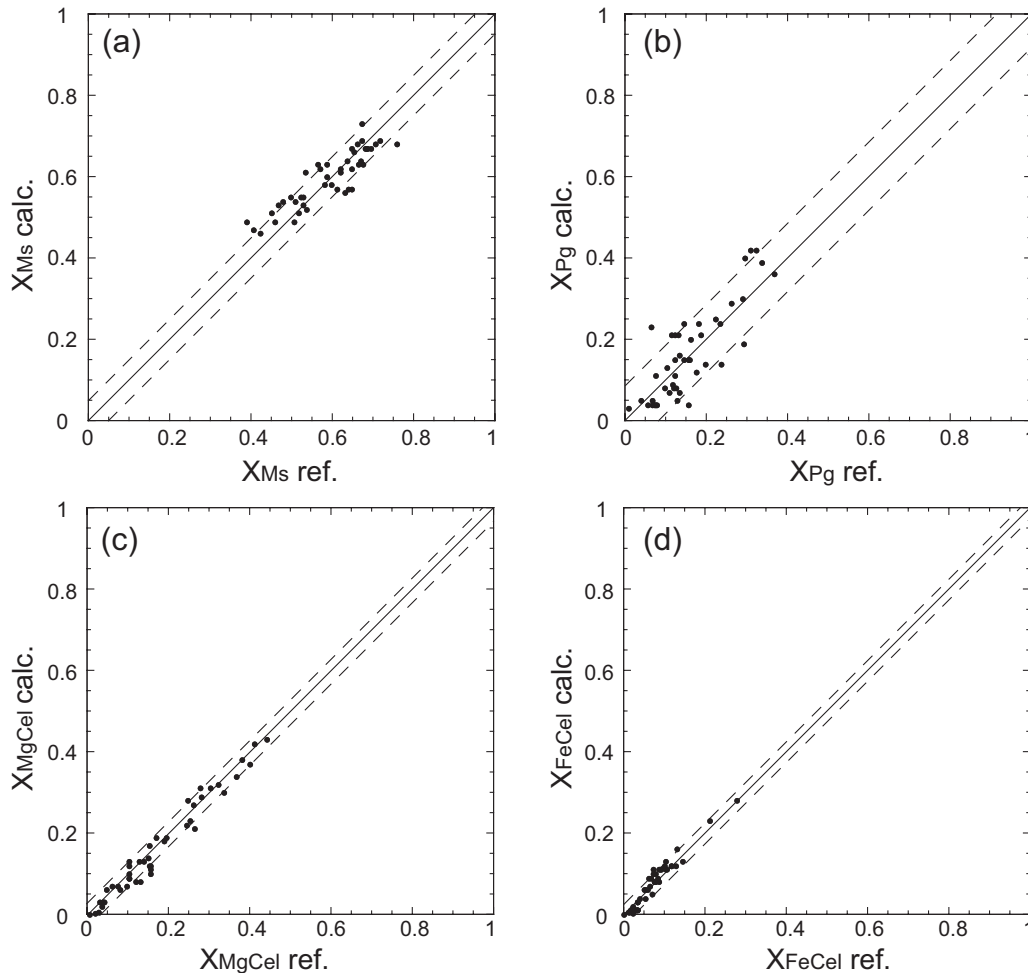
Fig. 4. Calculated end-member compositions of phengite vs reference compositions [(X_{Ms}ref, X_{Pg}ref, X_{MgCel}ref and X_{FeCel}ref) vs (X_{Ms}calc, X_{Pg}calc, X_{MgCel}calc and X_{FeCel}calc)]. The compositions are calculated at the reference *P–T* conditions of each coexisting phengite and paragonite pair for the bulk composition corresponding to a 1:1 mixture of the measured compositions of the coexisting phengite and paragonite. The dashed line is 2σ of the deviation between the calculated and the reference end-member compositions. (a) Calculated muscovite content vs reference muscovite content (2σ = 0·05). (b) Calculated paragonite content vs reference paragonite content (2σ = 0·08). (c) Calculated Mg-celadonite content vs reference Mg-celadonite content (2σ = 0·03). (d) Calculated Fe-celadonite content vs reference Fe-celadonite content (2σ = 0·02).

of Guidotti *et al.* (1994*b*) we calculated three binary *T–X* sections through the ternary solvus. These sections were calculated with the program DOMINO (De Capitani & Brown, 1987; De Capitani, 1994) for the reference pressure of 7 kbar given by Guidotti *et al.* (1994*b*) for their solvus. DOMINO is based on the THERIAK algorithm (De Capitani & Brown, 1987). The locations of the *T–X* sections are shown in Fig. 6b. A constant Si content in Phe is achieved by calculating the *T–X* sections on sections of constant X_{MgCel} (Fig. 6b). The Pg limb is calculated on sections with the end-members of ideal Pg and Phe (Fig. 6b). For a celadonite (MgCel) content in the range of 0·05–0·15 (Si 3·05–3·15 p.f.u.) there is good agreement between the data of Guidotti *et al.* (1994*b*) and the model presented here in the location of the Pg limb (Fig. 6a). In addition, there is good agreement

between the Ms limb of the solvus of Guidotti *et al.* (1994*b*) and the Ms limb of our model corresponding to a celadonite (MgCel) content of 0·15 (Fig. 6a).

Up to now, the only thermodynamic considerations that account for the effect of the celadonite component in Phe are those of Coggon & Holland (2002) for the system Na$_2$O–K$_2$O–MgO–Al$_2$O$_3$–SiO$_2$–H$_2$O. Those workers proposed 52 kJ to be the interaction energy on the binary Pg–MgCel join. This high interaction energy causes a miscibility gap on the binary Pg–MgCel join, which is very wide over a large *P–T* range and thus may restrict the position and shape of the ternary solvus to within a relatively small compositional range. In contrast, our investigations point to a much lower interaction energy (≈20 kJ at 10 kbar), and thus to a smaller miscibility gap on the binary Pg–MgCel join. Despite this
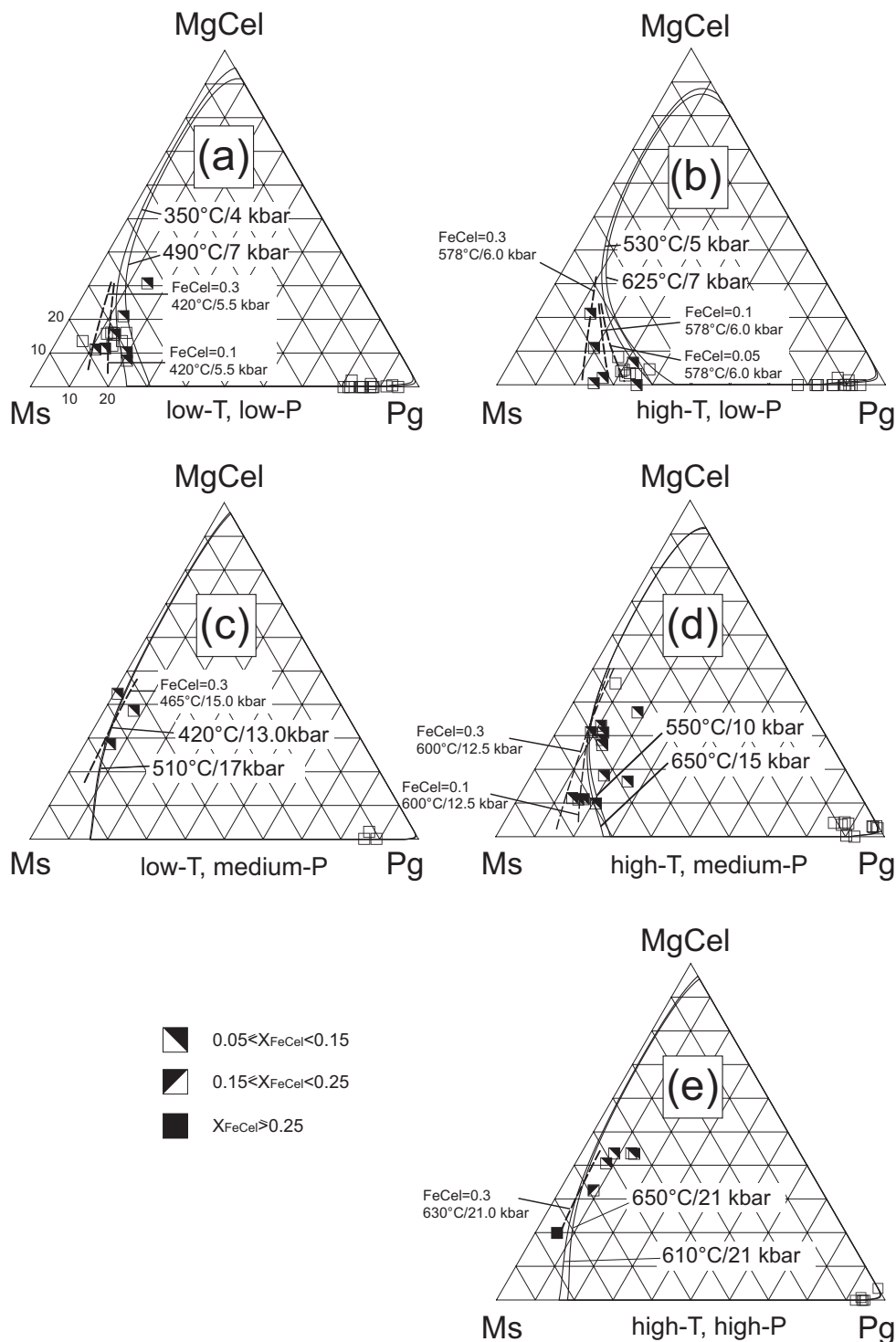
Fig. 5. Comparison of the ternary Ms–MgCel–Pg solvi, calculated from our model, with the natural data for coexisting phengite–paragonite pairs. The data are subdivided into five P, T-dependent categories according to Table 1: (a) low-T, low-P; (b) high-T, low-P; (c) low-T, medium-P; (d) high-T, medium-P; (e) high-T, high-P. Dashed lines indicate sectional parts of the quaternary Phe–Pg solvus. These sections are calculated for a constant X_{FeCel} in phengite and at P–T conditions lying between the lower and upper P–T boundaries of the P–T categories and are projected onto the ternary plane.
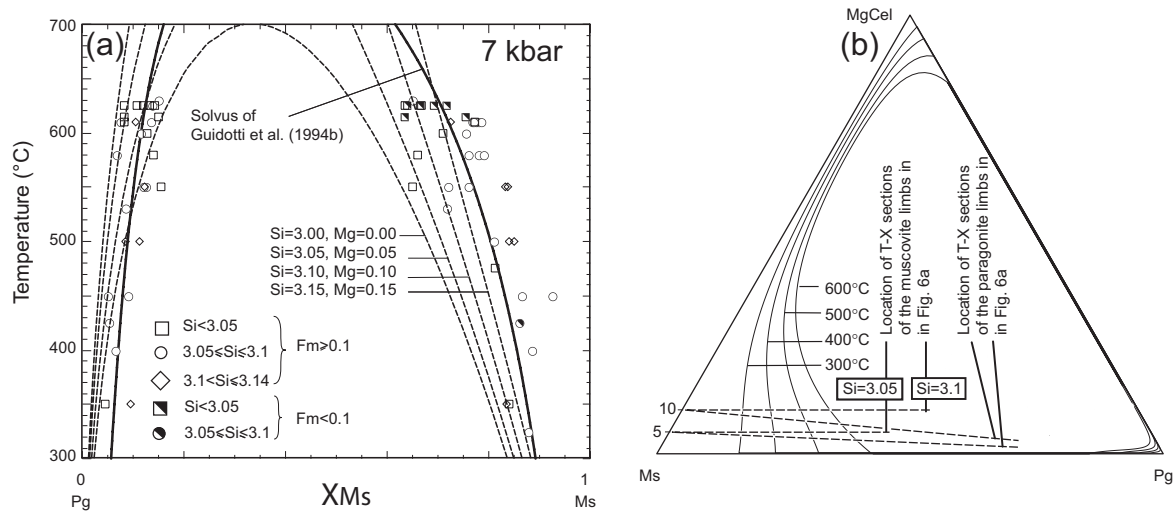
Fig. 6. (a) Comparison of the solvus of Guidotti *et al.* (1994*b*) with *T*–*X* sections through the ternary solvus calculated for Si content in phengite of 3·0, 3·05, 3·1 and 3·15 at the reference pressure of 7 kbar given by Guidotti *et al.* (1994*b*) for their solvus. The data points correspond to the compilation of Guidotti *et al.* (1994*b*), and the compositions are close to the muscovite–paragonite join. The data points are subdivided according to the Si and ferromagnesian content of the phengite. (b) Ternary solvi calculated at 300°C, 400°C, 500°C and 600°C at 7 kbar showing the location of the *T*–*X* sections. It should be noted that for a constant Si content in phengite the *T*–*X* sections cannot be calculated on a section between ideal paragonite and phengite.

relative small miscibility gap the solution model presented here predicts very low celadonite contents in paragonite for the compositions of natural coexisting phengite–paragonite pairs (Figs 5 and 6b). To compare the results obtained by Coggon & Holland (2002, fig. 5b) with our model we calculated *T*–*X* sections through the ternary Ms–MgCel–Pg solvus. These were calculated for different Si contents in Phe. In general, there is agreement between the results of Coggon & Holland (2002, fig. 5b) and our model (Fig. 7). However, by comparing the Ms limbs of our model with the Ms limbs of the model of Coggon & Holland (2002) it is obvious that the latter are restricted to a relatively small compositional range, particularly at higher Si (>3·2) content in Phe (Fig. 7). As stated above, this is caused by the high interaction energy on the Pg–MgCel join.

Limits of the presented solution model

Because the model is calibrated for pressures up to 21 kbar at about 650°C we do not recommend an extrapolation towards much higher pressures. At low pressures and high temperatures the solution model allows complete mixing between Pg–Ms and between Pg–Cel (MgCel, FeCel). As this occurs outside the high-temperature low-pressure stability limit of paragonite, which may be given by the assemblage phengite + paragonite + sillimanite + quartz (Grambling, 1984; see Guidotti, 1984 for further discussion), complete mixing on the above binary joins is regarded as a mathematical artefact of our model.
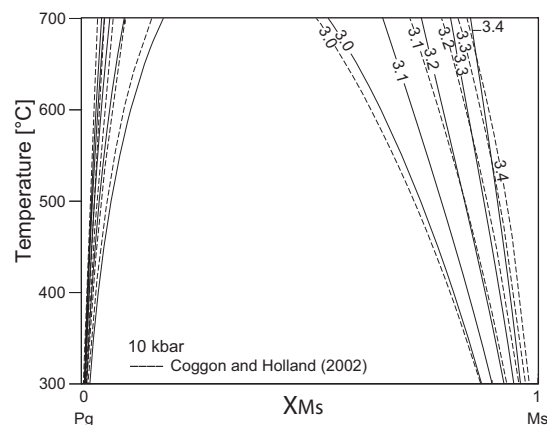

Fig. 7. Comparison of the solvi of Coggon & Holland (2002) with *T*–*X* sections through the ternary solvus calculated for Si content in phengite of 3·1, 3·2, 3·3 and 3·4 at pressure of 10 kbar. The location of the *T*–*X* sections is defined as in Fig. 6b.

Application

It is well known that the compositions of phengite in pelitic rocks are affected by the metamorphic conditions (Guidotti, 1973, 1984; Guidotti & Sassi, 1976, 1998). To test whether our model predicts the compositional trends observed in Phe of pelitic rocks, we calculated the equilibrium phase diagram section (Fig. 8) and the end-member isopleths of phengite (Fig. 9) for the bulk composition corresponding to the average of 18 pelitic rock samples described by Shaw (1956) (in wt %: SiO_2
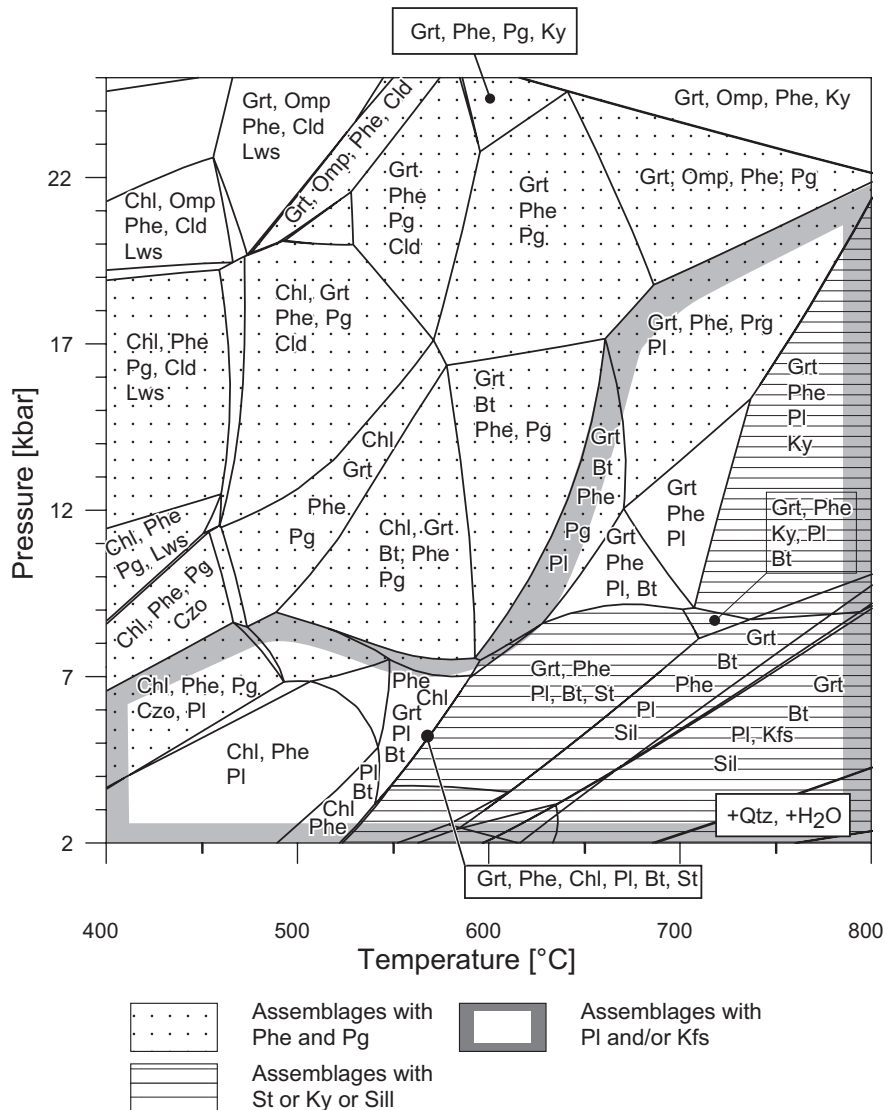
Fig. 8. Equilibrium phase diagram computed for an average pelitic bulk-rock composition. The diagram is calculated with the program DOMINO (De Capitani, 1994) and it postulates distinct stable phase assemblages and corresponding mineral compositions and mineral abundances based on thermodynamic properties defined in the database of Berman (1988, update 1992). Bulk-rock chemistry is normalized to 100 cations and all iron is taken as Fe^{2+}. Water ($a_{H_2O} = 1 \cdot 0$) and quartz are stable with all mineral assemblages. The stippled area outlines assemblages where phengite coexists with paragonite; the area outlined with a grey border corresponds to assemblages where feldspar is stable; the horizontal ruled area outlines assemblages where staurolite, kyanite or sillimanite is stable. Mineral abbreviations are after Kretz (1983).

61·37, TiO_2 0·98, Al_2O_3 19·25, FeO 6·91, MnO 0·7, MgO 2·03, CaO 0·46, Na_2O 1·3, K_2O 3·58). Nagel *et al.* (2002) also used this composition to discuss aspects of phase relations concerning metapelites, which experienced decompression from eclogite-facies conditions to amphibolite-facies conditions. The calculation was performed in the system K_2O–Na_2O–CaO–FeO–MgO–Al_2O_3–SiO_2–H_2O with DOMINO (De Capitani & Brown, 1987; De Capitani, 1994) using the database of Berman (1988, update 1992). For staurolite and chloritoid we used the thermodynamic data of Nagel *et al.* (2002). For garnet we used the solution model of

Berman (1990), for biotite binary (Phl, Ann) ideal mixing on site (3) was assumed, for chlorite the solution model of Hunziker (2003) was used, for feldspar we used the solution model of Fuhrman & Lindsley (1988), for staurolite the solution model of Nagel *et al.* (2002), and for omphacite we used the model of Meyre *et al.* (1997). The activity of H_2O was assumed to be unity.

Figure 8 presents the equilibrium phase diagram section and Fig. 9a–d shows the corresponding compositional variation of Phe given by its end-member isopleths. The stippled area in the above figures represents the *P–T* field where Pg and Phe coexist.
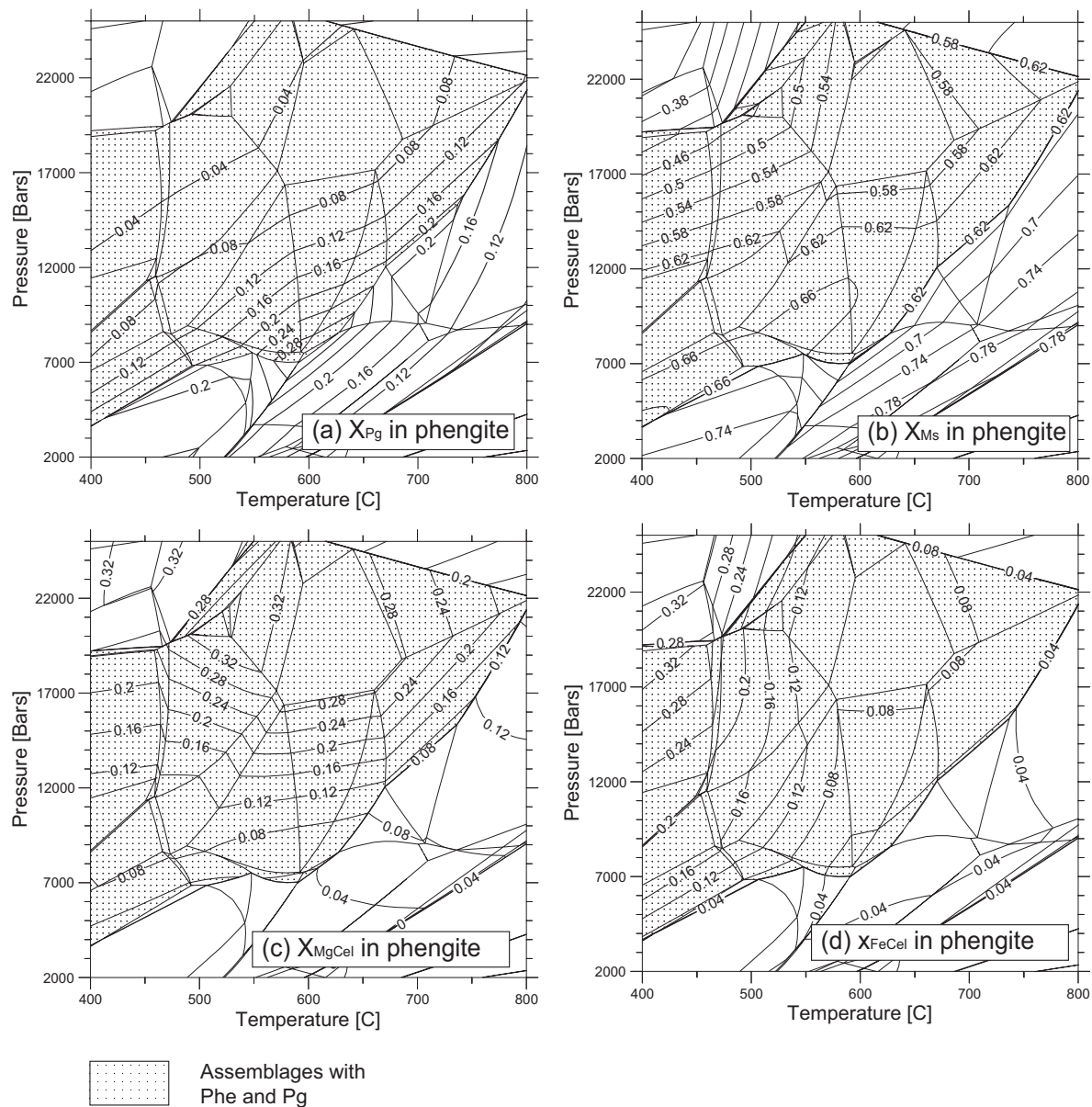
Fig. 9. *P–T* diagrams showing end-member isopleths of phengite computed for the same average pelitic bulk-rock composition as in Fig. 8. The diagram is calculated with the program DOMINO (De Capitani, 1994) based on the solution model presented here and on thermodynamic properties defined in the database of Berman (1988, update 1992). The stippled area outlines assemblages where phengite coexists with paragonite. (a) Paragonite content in phengite. (b) Muscovite content in phengite. (c) Mg-celadonite content in phengite. (d) Fe-celadonite content in phengite.

Effects of pressure and temperature on the composition of phengite

From Fig. 9a it can be seen that as temperature and pressure increases Phe becomes Na enriched up to $\approx 0.3 X_{Pg}$ in phengite. Further temperature and pressure increase has the opposite effect as the Na content decreases and the K content increases in Phe (Fig. 9a and b). The conditions of maximum Na content in Phe are shifted towards higher temperatures as pressure increases. At the same time the maximum amount of Na decreases (see also Guidotti & Sassi, 1976, fig. 13). Because the Phe–Pg solvus widens in response to both a pressure increase and an increase of the celadonite content in Phe, the maximum Na content in Phe decreases as pressure increases. The *P–T* conditions of maximum Na content in Phe are defined by the low-pressure stability limit of Pg at temperatures higher than about 600°C (Figs 8 and 9a). Similar compositional trends were

described by Guidotti & Sassi (1976, figs 7, 13 and 14). At high-T and low-P conditions within the stability range of phases such as St, Ky and sillimanite (Sil) (Fig. 8, area with horizontal ruling) the Na content in Phe decreases as temperature increases and increases as pressure increases (Fig. 9a). The thermally induced decrease of the Na content in Phe is probably caused by the breakdown of Na-rich Phe, which releases Al, forms Pl and produces K-enriched Phe [Guidotti & Sassi, 1976, reaction (7)]. This is in accordance with our calculation as the abundance of Phe decreases within the stability fields of St, Ky and Sil (Keller *et al.*, 2005).

The equilibrium diagram (Fig. 8) predicts that the thermally driven reaction progress, forming high Al phases so typical for the progressive Barrow-type metamorphism, may occur in very small T intervals where continuous and discontinuous reactions take place (e.g. breakdown of Chl and St). However, in collision mountain belts, the formation of high-Al phases may occur during approximately isothermal decompression from high-pressure conditions, which has recently been discussed for the central Alps (Lepontine Dome) by Nagel *et al.* (2002) [see Keller *et al.* (2005) for further discussion].

Figure 9c and d shows the P–T-induced variation of the celadonite content. The isopleths of the MgCel content in Phe are predominantly functions of pressure within most assemblages, whereas the FeCel content in Phe decreases as temperature increases, particularly at higher pressures (Fig. 9c and d). By combining the compositional variation of the two celadonite end-members the variation of the celadonite content coincides with that discussed by Guidotti & Sassi (1976, fig. 12). Those workers stated that: (1) particularly at low temperatures the celadonite content increases as pressure increases; (2) particularly at higher pressures the celadonite content decreases as temperature increases. By comparing the isopleths of X_{FeCel} in Phe with calculated abundance of Grt it is indicated that the FeCel content in Phe probably decreases during thermally driven growth of Grt (see Keller *et al.*, 2005).

CONCLUSION

We believe that our model represents an improvement over existing solution models for white micas as it accounts for the effect of the celadonite component on the Phe–Pg solvus. When the model is used to calculate the P–T-dependent compositional variation of Phe in multicomponent systems, it gives reasonable and consistent results, in both quantitative and qualitative respects, at least for metapelites. The model should be particularly useful in modelling the phase relations and corresponding white mica composition for distinct pelitic bulk compositions, particularly for high-grade metamorphic conditions where the white micas can usually be described in terms of the end-members Ms, Pg, MgCel and FeCel.

REFERENCES

Ahn, J., Peacor, D. R. & Essene, E. J. (1985). Coexisting paragonite–phengite in blueschist eclogite: a TEM study. *American Mineralogist* **70**, 1193–1204.

Ashworth, J. R. & Evirgen, M. M. (1984). Garnet and associated minerals in the southern margin of the Menderes Massif, southwest Turkey. *Geological Magazine* **121**, 323–337.

Berman, R. G. (1988). Internally-consistent thermodynamic data for minerals in the system Na_2O–K_2O–CaO–FeO–Fe_2O–Al_2O_3–SiO_2–H_2O–CO_2. *Journal of Petrology* **29**, 445–552.

Berman, R. G. (1990). Mixing properties of Ca–Mg–Fe–Mn garnets. *American Mineralogist* **75**, 328–344.

Blencoe, J. G., Guidotti, C. V. & Sassi, F. P. (1994). The paragonite–muscovite solvus: II. Numerical geothermometers for natural, quasibinary paragonite–muscovite pairs. *Geochimica et Cosmochimica Acta* **58**, 2277–2288.

Bousquet, R., Goffé, B., Oberhänsli, R. & Patriat, M. (2002). The tectono-metamorphic history of the Valaisan domain from the Western to the Central Alps: new constraints on the evolution of the Alps. *Geological Society of America Bulletin* **114**, 207–225.

Brown, E. H. & Forbes, R. B. (1986). Phase petrology of the eclogitic rocks in the Fairbanks district, Alaska. In: Evans, B. W. & Brown, E. H. (eds) *Blueschists and Eclogites. Geological Society of America, Memoirs* **164**, 155–167.

Chatterjee, N. D. & Flux, S. (1986). Thermodynamic mixing properties of muscovite–paragonite crystalline solutions at high temperatures and pressures, and their geological applications. *Journal of Petrology* **27**, 677–693.

Chatterjee, N. D. & Froese, E. (1975). A thermodynamic study of the pseudobinary join muscovite–paragonite in the system $KAlSi_3O_8$–$NaAlSi_3O_8$–Al_2O_3–SiO_2–H_2O. *American Mineralogist* **60**, 985–993.

Chopin, C. (1979). De la Vanois au massif du Grand Paradis, une approche pétrographique et radiochronologique de la signification géodynamique du métamorphisme de haute pression. Ph.D. thesis, Université de Paris VI, 145 pp.

Chopin, C., Henry, C. & Michard, A. (1991). Geology and petrology of the coesite-bearing terrain, Dora Maira massif, Western Alps. *European Journal of Mineralogy* **3**, 263–291.

Coggon, R. & Holland, T. J. B. (2002). Mixing properties of phengitic micas and revised garnet–phengite thermobarometers. *Journal of Metamorphic Geology* **20**, 683–696.

De Capitani, C. (1994). Gleichgewichts-Phasendiagramme: Theorie und Software. *Berichte der Deutschen Mineralogischen Gesellschaft. Beihefte zum European Journal of Mineralogy* **6**, 48.

De Capitani, C. & Brown, T. H. (1987). The computation of chemical equilibrium in complex systems containing non-ideal solutions. *Geochimica et Cosmochimica Acta* **51**, 2639–2652.

Enami, M. (1983). Petrology of pelitic schists in the oligoclase–biotite zone of the Sanbagawa metamorphic terrain, Japan: phase equilibria in the highest grade zone of a high-pressure intermediate type of metamorphic belt. *Journal of Metamorphic Geology* **1**, 141–161.

Eugster, H. P., Albee, A. L., Bence, A. E., Thompson, J. B. & Waldbaum, D. R. (1972). The two-phase region and excess mixing properties of paragonite–muscovite crystalline solutions. *Journal of Petrology* **13**, 147–179.

Feininger, T. (1980). Eclogite and related high-pressure regional metamorphic rocks from the Andes of Ecuador. *Journal of Petrology* **21**, 107–140.

Ferry, J. M. (1992). Regional metamorphism of the Waits River Formation, Eastern Vermont: delineation of a new type of giant hydrothermal system. *Journal of Petrology* **33**, 45–94.

Franceschelli, M., Mellini, M., Memmi, I. & Ricci, C. A. (1989). Sudoite, a rock-forming mineral in Verrucano of the northern Apennines (Italy) and the sudoite–chloritoid–pyrophyllite assemblage in prograde metamorphism. *Contributions to Mineralogy and Petrology* **101**, 274–279.

Franz, C. & Althaus, E. (1976). Experimental investigation on the formation of solid solutions in sodium–aluminum–magnesian micas. *Neues Jahrbuch für Mineralogie, Abhandlungen* **126**, 233–253.

Fuhrman, M. L & Lindsley, D. H. (1988). Ternary-feldspar modelling and thermometry. *American Mineralogist* **73**, 201–215.

Gil Ibarguchi, J. I. & Dallmeyer, R. D. (1991). Hercynian blueschist metamorphism in north Portugal: tectonothermal implications. *Journal of Metamorphic Geology* **9**, 539–549.

Grambling, J. A. (1984). Coexisting paragonite and quartz in sillimanite rocks from New Mexico. *American Mineralogist* **69**, 79–87.

Guidotti, C. V. (1973). Compositional variation of muscovite as a function of metamorphic grade and assemblages in metapelites from N. W. Maine. *Contributions to Mineralogy and Petrology* **42**, 33–42.

Guidotti, C. V. (1984). Micas in metamorphic rocks. In: Bailey, S. W. (ed.) *Micas. Mineralogical Society of America. Reviews in Mineralogy* **13**, 357–467.

Guidotti, C. V. & Sassi, F. P. (1976). Muscovite as a petrogenetic indicator mineral in pelitic schists. *Neues Jahrbuch für Mineralogie, Abhandlungen* **127**, 97–142.

Guidotti, C. V. & Sassi, F. P. (1998). Petrogenetic significance of Na–K white mica mineralogy: recent advances for metamorphic rocks. *European Journal of Mineralogy* **10**, 815–854.

Guidotti, C. V., Sassi, F. P., Sassi, R. & Blencoe, J. G. (1994*a*). The effects of ferromagnesian components on the paragonite–muscovite solvus: a semiquantitative analysis based on chemical data for the natural paragonite–muscovite pairs. *Journal of Metamorphic Geology* **12**, 779–788.

Guidotti, C. V., Sassi, F. P., Blencoe, J. G. & Selverstone, J. (1994*b*). The paragonite–muscovite solvus: I. *P–T–X* limits derived from the Na–K composition of natural, quasibinary paragonite–muscovite pairs. *Geochimica et Cosmochimica Acta* **58**, 2269–2275.

Guidotti, C. V., Sassi, F. P., Comodi, P., Zanazzi, P. F. & Blencoe, J. G. (2000). The contrasting response of muscovite and paragonite to increasing pressure: petrological implications. *Canadian Mineralogist* **38**, 707–712.

Heinrich, C. A. (1982). Kyanite-eclogite to amphibolite facies evolution of hydrous mafic and pelitic rocks, Adula nappe, Central Alps. *Contributions to Mineralogy and Petrology* **81**, 30–38.

Hirajima, T., Shohei, B., Yoshikuni, H. & Yoshihide, O. (1988). Phase petrology of eclogites and related rocks from the Motalafiella high-pressure metamorphic complex in Spitsbergen (Arctic Ocean) and its significance. *Lithos* **22**, 75–97.

Höck, V. (1974). Coexisting phengite, paragonite and margarite in metasediments of the Mittlere Hohe Tauern, Austria. *Contributions to Mineralogy and Petrology* **43**, 261–273.

Hoffer, E. (1978). On the 'late' formation of paragonite and its breakdown in pelitic rocks of the southern Damara orogen (Namibia). *Contributions to Mineralogy and Petrology* **67**, 209–219.

Hunziker, P. (2003). The stability of tri-octahedral Fe^{2+}–Mg–Al chlorite. A combined experimental and theoretical study. Ph.D. thesis, University of Basel, 162 pp.

Irouschek, A. (1983). Mineralogie und Petrographie von Metapeliten der Simano-Decke unter besonderer Berücksichtigung Cordieritführender Gesteine. Ph.D. thesis, University of Basel, 205 pp.

Jackson, S. L. (1989). Extension of Wohl's ternary asymmetric solution model to four and *n* components. *American Mineralogist* **74**, 14–17.

Katagas, C. & Baltatzis, E. (1980). Coexisting celadonite muscovite and paragonite in chlorite zone metapelites. *Neues Jahrbuch für Mineralogie, Monatshefte H* **5**, 206–214.

Keller, L. M., Abart, R., Schmid, S. M. & De Capitani, C. (2005). Phase relations and chemical composition of phengite and paragonite in pelitic schists during decompression: a case study from the Monte Rosa nappe and Camughera–Moncucco unit, Western Alps. *Journal of Petrology* **46**, doi:10.1093/petrology/egi051.

Koch, E. (1982). Mineralogie und plurifazielle Metamorphose der Pelite in der Adula-Decke (Zentralalpen). Ph.D. thesis, University of Basel, 201 pp.

Kretz, R. (1983). Symbols for rock-forming minerals. *American Mineralogist* **68**, 277–279.

Massonne, H. J. & Szpurka, Z. (1997). Thermodynamic properties of white micas on the basis of high-pressure experiments in the system $K_2O–MgO–Al_2O_3–SiO_2–H_2O$ and $K_2O–FeO–Al_2O_3–SiO_2–H_2O$. *Lithos* **41**, 229–250.

Meyre, C., De Capitani, C. & Partsch, J. H. (1997). A ternary solid solution model for omphacite and its application to geothermobarometry of eclogites from the middle Adula nappe (Central Alps, Switzerland). *Journal of Metamorphic Geology* **15**, 687–700.

Meyre, C., De Capitani, C., Zack, T. & Frey, M. (1999). Petrology of high-pressure metapelites from the Adula nappe (Central Alps, Switzerland). *Journal of Petrology* **40**, 199–213.

Nagel, T. (2002). Metamorphic and structural history of the southern Adula nappe (Graubünden, Switzerland). Ph.D. thesis, University of Basel, 103 pp.

Nagel, T., De Capitani, C. & Frey, M. (2002). Isograds and *P–T* evolution in the Southeastern Lepontine Dome (Graubünden, Switzerland). *Journal of Metamorphic Geology* **20**, 309–324.

Okay, A. I. (1989). An exotic eclogite/blueschist slice in a barrovian-style metamorphic terrain, Alanya Nappes, Southern Turkey. *Journal of Petrology* **30**, 107–132.

Roux, J. & Hovis, G. L. (1996). Thermodynamic mixing models for muscovite–paragonite solutions based on solution calorimetric and phase equilibrium data. *Journal of Petrology* **37**, 1241–1254.

Schmid, R., Wilke, M., Oberhänsli, R., Janssens, K., Falkenberg, G., Franz, L. & Gaab, A. (2003). Micro-XANES determination of ferric iron and its application in thermobarometry. *Lithos* **70**, 381–392.

Shaw, D. M. (1956). Geochemistry of pelitic rocks. Part 3: Major elements and general geochemistry. *Geological Society of America Bulletin* **67**, 919–934.

Theye, T. & Seidel, E. (1991). Petrology of low-grade high-pressure metapelites from the external Hellenides (Crete, Peloponnese) a case study with attention to sodic minerals. *European Journal of Mineralogy* **3**, 343–366.

Thompson, J. B. (1957). The graphical analysis of the mineral assemblages in pelitic schists. *American Mineralogist* **42**, 842–858.

Thompson, J. B. & Thompson, A. B. (1976). A model system for mineral facies in pelitic schists. *Contributions to Mineralogy and Petrology* **58**, 243–277.

Vidal, O., Para, T. & Trotet, F. (2001). A thermodynamic model for Fe–Mg aluminous chlorite using data from phase equilibrium experiments and natural pelitic assemblages in the 100°C to 600°C, 1 to 25 kb range. *American Journal of Science* **301**, 557–592.

Wohl, K. (1946). Thermodynamic evaluation of binary and ternary liquid systems. *Transactions of the American Institute of Chemical Engineers* **42**, 215–249.

Wohl, K. (1953). Thermodynamic evaluation of binary and ternary liquid systems. *Chemical Engineering Progress* **49**, 218–219.

Zhang, R. & Liou, J. G. (1994). Coesite-bearing eclogite in Henan Province, central China: detailed petrography, glaucophane stability and *P–T* path. *European Journal of Mineralogy* **6**, 217–233.